# VERIFICATION OF NONLINEAR FINITE ELEMENT MODELLING OF I-SHAPED STEEL BEAMS UNDER COMBINED LOADING

## Muharrem AKTAŞ*

*Özet* – Ekonomik zorluklar ve laboratuvar imkanlarının kısıtlı olmasından dolayı gerçek deneyler yerine sonlu elemanlar yöntemi kullanılarak bilgisayar programında sayısal deneyler yapılabilir. Bu çalışmada aynı anda zayıf eksen altında eğilmeye ve eksenel basınç kuvvetine maruz kalmış I-kesitli çelik kirişlerin sonlu elemanlar yöntemi ile hesap yapan Abaqus 6.3 adlı bilgisayar programı ile modellenmesi yapılmıştır. Yapılan modelin doğruluğu gerçek laboratuvar deney sonuçlarıyla kıyaslanarak test edilmiştir. Bu makalede modelleme basamakları, kullanılan paket programın özellikleri ve sonlu elemanlar modelinin aşamaları ile yapılan kabuller detaylı olarak sunulmuştur.

*Anahtar Kelimeler* – Lineer olmayan davraniş, sonlu elaman yöntemi, zayıf eksen altında eğilme, karşılıklı etkileşim diyagramı, plastisite

*Abstract* – Experimental testing is expensive and time consuming to perform large series of tests. The other choice is to use a numerical experimental series with the help of a computer by using nonlinear finite element software. Given the reliance of the present work on this analytical method, it is important to clearly state the modeling approached used, software packages employed, and any assumptions made during the construction of the finite element analogs for the I-shaped cross-sections under investigation. In addition, verification of the modeling techniques against full-scale experimental testing can be of great value. The commercial finite element software package ABAQUS 6.3 is employed in this research. All modeling reported herein considers both nonlinear geometric and material influences.

*Key Words* – Nonlinear behavior, finite element modelling, minor axis bending, interaction diagrams, plasticity, I-beams.

*SA.Ü Mühendislik Fakültesi, İnşaat Mühendisliği Bölümü, Adapazarı

## I. INTRODUCTION

Experimental testing is the best way to investigate the behavior of structures. However, it is expensive and time consuming to perform the large series of tests needed to investigate such desired effect. The other choice is to use a numerical experimental series with the help of a computer to perform the required parametric studies. Such numerical experiments rely on accurate computer models of the structures. The nonlinear finite element program, ABAQUS, is employed in this research. In non linear finite element analysis techniques, assumptions related to the type of stress strain curve, boundary conditions, initial imperfection etc. may impact on the quality of the numerical results.

For verification purpose, experiments done by Rasmussen and Chick [10] at 1995 are used. This experimental research program focuses on the study of I-shaped members possessing slender cross-sectional profiles subjected to combined loading applied in a proportional fashion. As part of this Australian research, the extreme case of pure minor axis bending as well as the cases where the interaction of minor axis bending with axial loading are considered and thus valuable experimental results are contained in this work; vis-à-vis a verification study related to the present research.

Nonlinear finite element modeling is at the heart of the research work reported on in the current study. Given the reliance of the present work on this analytical method, it is important to clearly state the modeling approached used, software packages employed, and any assumptions made during the construction of the finite element analogs for the I-shaped cross-sections under investigation. In addition, verification of the modeling techniques against full-scale experimental testing can be of great value.

The commercial multipurpose finite element software package ABAQUS version 6.3 is employed in this research. All modeling reported herein considers both nonlinear geometric and material influences.

The I-shaped cross-sections considered in the current research employ shell finite elements positioned along the

middle surfaces on the cross-sectional constituent plate components. The following sub-sections endeavor to meet the above requirements and lead to a clear understanding of the approach, and subsequent limitations, of the present work.

## II. NONLINEARITIES IN STRUCTURAL RESPONSE

### Sources of nonlinearities

structural analysis there are three sources of nonlinearities in analysis. The corresponding nonlinear are identified by the terms material, geometric and boundary conditions. All modeling reported herein considers both nonlinear geometric and material sources.

*Material Nonlinearity:* The stress-strain curve of steel is elastic until some significant point called the yielding point. After the attainment of the yield point, the strain curve becomes nonlinear and the strains are partially irrecoverable. In other words when the material behavior does not fit the elastic model ($E\varepsilon$) there is a phenomenon of material nonlinearity. Effects due to the constitutive equations (stress-strain relations) that are nonlinear, are referred to as material nonlinearities.

*Geometrical nonlinearity:* In elementary structural theory effect of deformations are neglected when writing the equations of equilibrium and motion. In other words the behavior is described with respect to the undeformed configuration. Real structures are in equilibrium in their deformed configuration, not their undeformed configuration, as implied by elementary structural theory. Especially when there is large deflection small strain geometric nonlinearity must be taken into account. Ignoring the effects of geometric nonlinearity makes the governing kinematic relationships linear and thus it is impossible to capture phenomena such as bifurcation buckling.

### II.2 Non Linear Finite Element Solution Algorithm

The objective of the nonlinear finite element analysis is to trace the non linear load-displacement path in multi-dimensional configuration space. In a non linear analysis, solving a single system of linear equations directly does not give the equilibrium condition related to physical system response. The loading must be defined as a function of time and nonlinear response obtained by incrementing time (in the case of a static analysis, time is a dummy variable associated with incremental loading of the structural system). In ABAQUS this simulation is achieved by breaking the total time into a number of time increments. ABAQUS then calculate the approximate equilibrium configuration at the end of each time increment via intermediate iterations carried out within each increment. Several solution algorithms are proposed and applied to trace the equilibrium path. Newton's method is the basic method, and many other algorithms are developed by modifying this method. However, Newton's method fails around the critical points; meaning it is unable to negotiate solution features at the interface between stable and unstable equilibrium conditions. One solution method for tracing the nonlinear equilibrium path that is used in ABAQUS in such instances is Riks-Wempner method.

The advantage of the Riks-Wempner method is its ability to trace behavior beyond a critical point. In other words, this technique permits limit points on the equilibrium path to be negotiated. The Riks-Wempner method is also sometimes referred to as the arc-length method. In arc-length methods, the solution is constrained to lie either in a plane normal to the tangent of the equilibrium path at the beginning of the increment or on a sphere with radius equal to the length of the tangent. This method allows tracing snap-through as well as snap-back behavior [9].

### II.3 Von Mises Metal Plasticity Model in ABAQUS

A yield criterion is a law which defines the limit of elastic behavior under any possible combination of stresses at a point in a given material. ABAQUS permits several different type of yield criteria, but the von Mises yield criterion is selected in this research because of its ability to accurately predict yielding in body centered cubic crystalline based metals such as steel [1].

When developing the mathematical model for a yield criterion some assumptions may be made. First, material may be assumed to be isotropic. Second, Bauschinger effect may be neglected. Third, uniform hydrostatic tension or compression does not have an effect on yielding [4]. A geometrical representation of the yield criterion in principal stress space is shown in Figure 1. The yielding only depends on the deviatoric stress vector OP. The elastic state of stress is defined as being any point inside the cylinder, and yielding is defined as any state of stress that permits the stress point to lie on the surface of the cylinder.
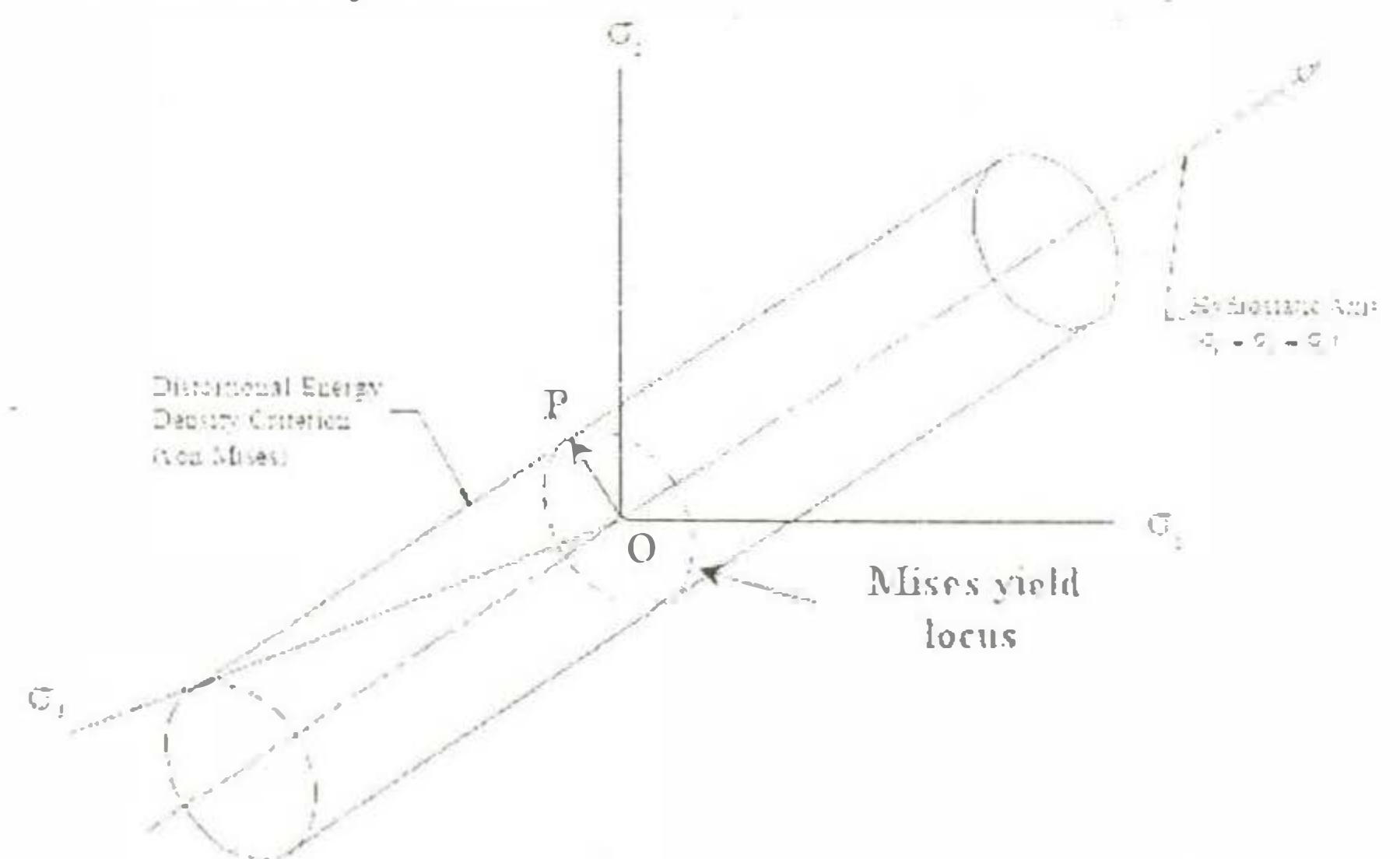


Figure 1 Yield surface in principal stress space

## II.4 Evolution of Failure Surface - Isotropic Hardening

Plastic deformations may continue after initial yield is reached, and this behavior may be accompanied by changes in the yield surface. The relationship for the post yield behavior of the material is known as the flow rule. When the material is loaded beyond a certain point the stress state reaches the yield surface making yield function zero at that point.

If the material is non hardening (i.e. perfectly plastic material) the yield surface does not change thus the stress point always lies on a surface formed by the locus of points corresponding to a constant yield stress. In other words incremental loading will either tend to reduce the value of the yield function below zero, which is also known as unloading, or incremental loading will tend to increase the value of yielding function above zero, which is not physically possible. In this case the stress point moves on the yield surface as the structure deforms plastically. If the material is strain hardening, yield surface evolves as the plastic deformation develops. In this case the yield surface expands or moves with the stress point still on the yield surface. To account for such changes the yield function must be generalized to define the subsequent yield surface configurations beyond the initial one. However, what will be the direction of the plastic flow must be answered.

In order to catch the real behavior of the material through analytical means, an appropriate plastic potential function should be picked. A plastic potential function can be chosen as the direction to cause maximum dissipation of plastic work.

The direction of plastic strain vector must be located perpendicular to the incremental stress vector. Having known that the stress state is on the yield surface the incremental stress vector must be tangent to the yield surface which makes plastic flow vector normal to the yield surface (Figure 2). Also the new plastic potential surface is now the yield surface. This choice of the flow rule, where the plastic straining is perpendicular to the yield surface is called associative flow rule.

Getting the maximum dissipation of plastic work by the associative flow rule is only valid for elastic-perfectly plastic materials. This flow rule may not give maximum plastic dissipation for many types of hardening material. However, it is very popular and widely used in the literature for its capability of capturing true behavior for a large variety of materials. Associated flow models give good results with the materials whose plastic flow is formed by dislocation motion when there are no sudden changes in the direction of the plastic strain rate at a point [1].

After reaching the yield point, many materials show an increase in stress with the increase in strain. Also after unloading and reloading the same material is seen to have increased its yield point. This response of the material is called the hardening response. Increase in the yield point also means increase in the yield surface. If the yield surface changes its size uniformly in all directions, such that the yield stress increases (or decreases) in all stress directions as plastic straining occurs, then the response is called isotropic hardening [1] (Figure 2).

Meaning that in the case of the von Mises yield surface, isotropic hardening is manifested through an evolution of the cylindrical yield surface in the three dimensional principal stress space such that on planes oriented orthogonally with the hydrostatic stress generator of the surface. The circular outline of the von Mises surface appears as a cylinder whose circumference increases, as the stress point continues to impinge on the yield surface during plastic flow, while the location of the center of the circle remains unchanged. In this research, isotropic hardening and the associated flow rule are adopted and used in conjunction with the ABAQUS software system.

## II.5 S4R Shell Element

The ABAQUS shell element library includes general purpose shell elements and specially formulated shell elements for thick and thin shell problems. In this study the S4R general purpose shell element is used to model the actual three dimensional geometry of the beam. This element is selected for use in the parametric study based on its satisfactory performance in the verification work described in the papers by Thomas and Earls and Greco and Earls[11,8].

In the S4R there are four nodes possessing 6 degrees of freedom per node. The general purpose shell elements give accurate solutions to most applications. S4R allows transverse shear deformation to be considered in a fashion that is consistent with Mindlin-Reissner theory. Also, it employs the discrete Kirchhoff techniques to provide satisfactory results as the shell thickness decreases [1].

Finite membrane strains are taken into account in the S4R formulation and thus the element admits changes in thickness as a function of membrane strain. Poisson's ratio of the section defines whether the shell thickness
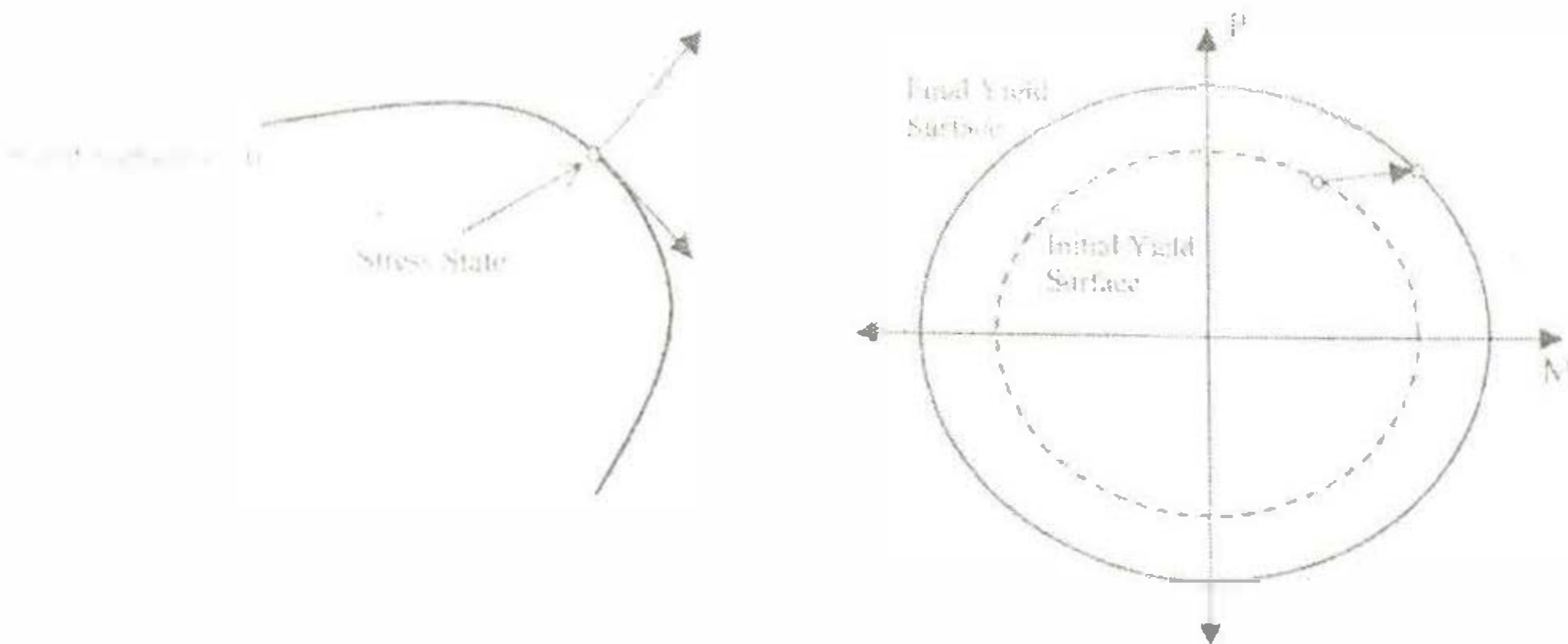


Figure 2 Normality of plastic strain and description of isotropic hardening.

changes as a function of the membrane strain or not. Setting the Poisson's ratio to zero will keep the shell thickness constant and will allow the elements fit for small strain large rotation analysis [1].

S4R formulation is based on a first order shear deformation theory. In other words the shell employs linear displacement and rotation interpolation in the context of Mindlin-Reissner theory, but the shear deformations are then obtained directly from a consideration of the nodal deformations. This approach is made to be consistent with the assumption that cross-sections remain plain but not normal to the Gauss surface of the shell.

ABAQUS uses a lower order quadrature rule, called reduced integration, to calculate the S4R element stiffness. A single integration point is used in this particular element. Reduced integration has two main advantages: it significantly reduces running time by using fewer sampling points; and with fewer sampling points, some of the more complicated displacement modes offer less resistance to deformation. This increases the accuracy of finite element analysis [5]. Sometimes using reduced integration yields element stiffness matrices that display one or more false zero energy mode, which may also be the cause of an unstable, or very inaccurate solution [4]. However; ABAQUS overcomes this problem by using hourglass control. Hourglass control assigns an artificial (and usually quite small) stiffness to the so-called drilling degree of freedom on the shell. This stiffness value depends on the factors usually given as a small fraction of typical shear modulus for material [1]

## III.    TEST SPECIMEN

### III.1 Geometry of the specimen

Rasmussen and Chick [10] had tested a series of thin walled I-beams in combined compression and minor axis bending. They focus on a single I-shaped cross-section whose nominal dimensions appear in figure 3.
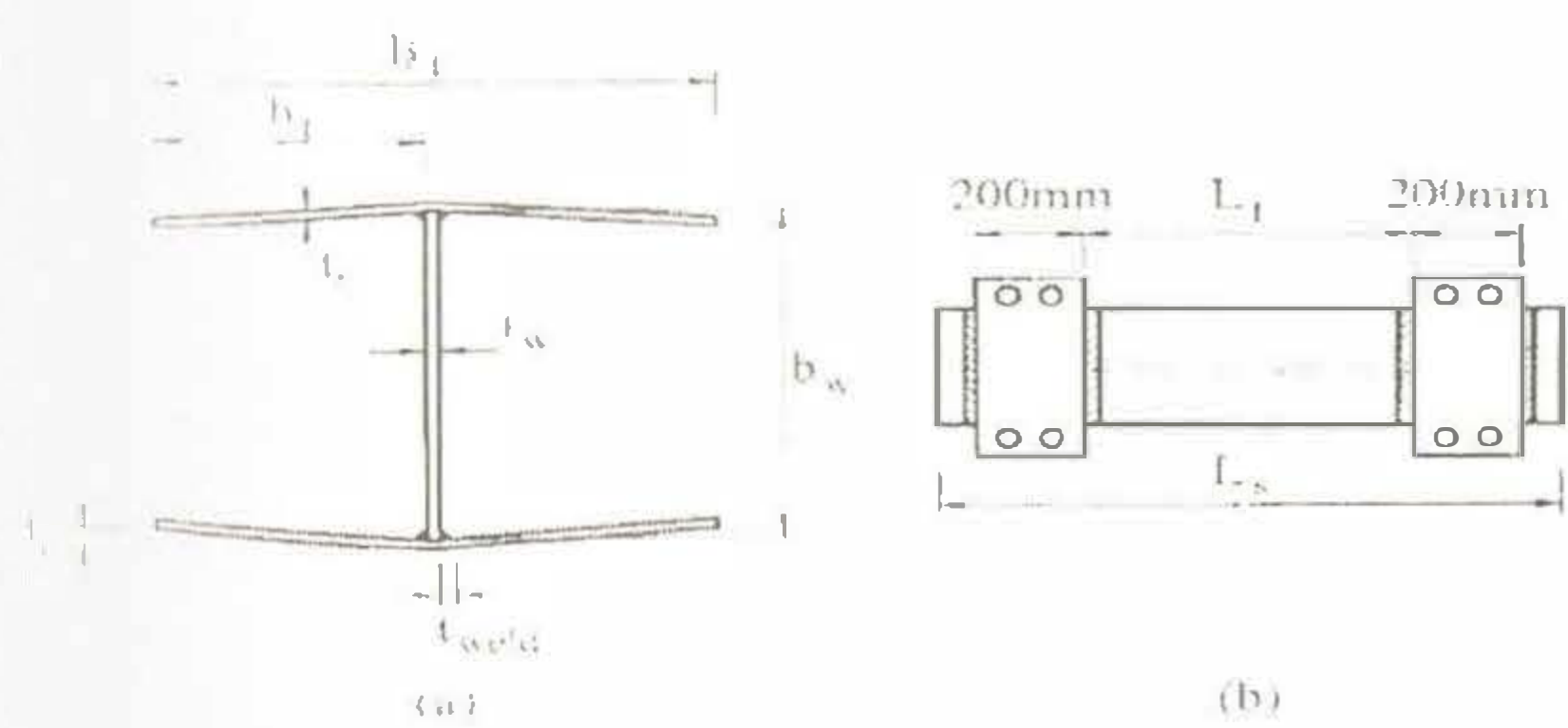


Figure 3 Nomenclature (Rasmussen and Chick, 1995)

Using this single cross-section, three distinct study cases are considered through the variation of the member unbraced length. Specifically, short (Lb = 800mm), medium (Lb = 3500mm), and long (Lb = 5800mm) members are treated in their work. In this study beams with 3500 mm and 5800 mm lengths from the research of

Rasmussen and Chick [10] are used to validate the finite modeling strategies for the investigation of interaction between axial loading and minor axis bending. The cross-section used in the experimental test was a slender I-section fabricated from high strength steel with $F_y = 350\ MPa$.

The measured cross-sectional dimensions, in addition to the ultimate forces applied to the models, are tabulated in table 1.

Table 1 Measured specimen lengths and applied loads

| Specimen | $t_f$ (mm) | $t_w$ (mm) | $b_w$ (mm) | $B_f$ (mm) | $f_c$ (mm) | $M$ (kNm) | $P$ (kN) |
|---|---|---|---|---|---|---|---|
| 3500-2 | 5.02 | 4.95 | 240.50 | 240.00 | 4.50 | 5.53 | 653 |
| 3500-3 | 4.97 | 4.98 | 240.00 | 239.50 | 6.50 | 9.57 | 553 |
| 3500-4 | 4.96 | 5.00 | 240.00 | 239.00 | 6.00 | 13.2 | 427 |
| 3500-5 | 5.01 | 5.00 | 240.50 | 239.50 | 4.50 | 39.63 | 65 |
| | | | | | | | |
| 5800-2 | 4.91 | 5.01 | 240.00 | 240.00 | 4.50 | 1.79 | 430 |
| 5800-3 | 4.99 | 5.01 | 241.00 | 240.00 | 5.00 | 7.26 | 318 |
| 5800-4 | 5.07 | 5.05 | 241.00 | 240.00 | 5.50 | 18.21 | 181 |

### III.2 Material Model

The behavior in the strain-hardening region is generally based on the nominal stress and engineering strain; which are calculated without considering the change in area of the cross-section. However, the change in the cross-sectional area of the specimen may be an important parameter when large deformations occur. In these cases the strain hardening range should be characterized using the true stress, obtained by dividing the load by the current area of the specimen. Nominal stress and strain data for uniaxial test for isotropic material can be converted into true stress and logarithmic plastic strain by using the following equations;

$$\sigma_{true} = \sigma_{nom}\left(1 + \varepsilon_{nom}\right) \qquad \varepsilon_{ln}^{pl} = \ln\left(1 + \varepsilon_{nom}\right) - \frac{\sigma_{true}}{E}$$

Rasmussen and Chick presented stress-strain properties of material loaded in tension in their report. Residual stresses are not included in this research since it is known to have no influence over the observed strength of hot-rolled structural members.

Uniaxial tension test results carried out under quasi-static conditions are adjusted to be static values according to the paper [7]. In that paper stress levels are decreased by 27.57 MPa because of the difference between the dynamic test loading and the actual static loading. Static yield stress is independent of testing procedure and the behavior of testing machine. Static yield stress is defined as the stress level when the strain rate is zero or when the

testing speed is zero [10]. In figure 4 difference between
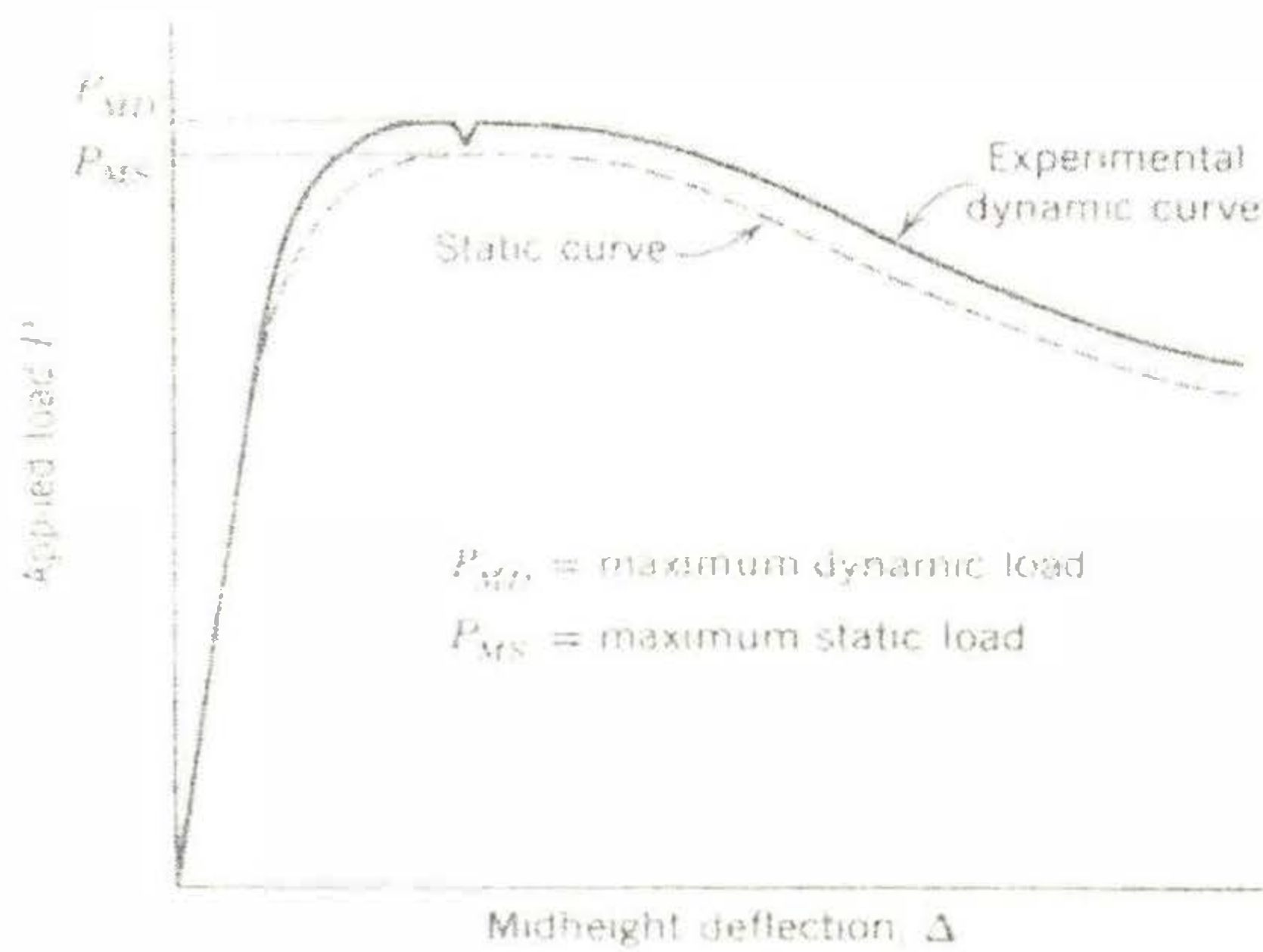static and dynamic loading can be seen.



Figure 4 Difference between dynamic loading and static loading [6]

The reported mechanical response values from coupon
testing appear in table 2 in engineering units; these are
subsequently adjusted to be static values and then
converted to an idealized multilinear true stress and
logarithmic strain format (see figure 4, table 3,4,5,6 and
7) prior to importation into the finite element software
package, ABAQUS. In table 2 $f_{yc}$ $f_{yt}$ and $f_{ut}$ are static
compressive yield stress, static tensile yield stress and
ultimate tensile stress, respectively.

Table 2 Mechanical properties

| Specimen | Plate | E (GPa) | $f_{yc}$ (MPa) | $f_{yt}$ (MPa) | $f_{ut}$ (MPa) |
|----------|-------|---------|---------------|---------------|---------------|
| 3500-2 | 6 | 204 | 457 | 431 | 503 |
| 3500-3 | 2 | 198 | 450 | 435 | 498 |
| 3500-4 | 3 | 200 | 453 | 436 | 506 |
| 3500-5 | 4 | 200 | 466 | 431 | 509 |
| 5800-2 | 1 | 199 | 451 | 435 | 502 |
| 5800-3 | 2 | 198 | 450 | 435 | 498 |
| 5800-4 | 1 | 199 | 451 | 435 | 502 |

Table 3 Stress- Strain values for Plate 1

| $\sigma_{nom}$ | $\varepsilon_{nom}$ | $\sigma_{true}$ | $\varepsilon_{ln}^{pl}$ |
|------|------|------|------|
| 435.5 | 0.002188 | 408.874 | 0 |
| 435.5 | 0.014904 | 414.4099 | 0.012567 |
| 503 | 0.063462 | 507.3492 | 0.05884 |
| 525 | 0.10875 | 554.5098 | 0.100305 |
| 525 | 0.186635 | 595.404 | 0.167991 |

Table 4 Stress -Strain values for Plate 2

| $\sigma_{nom}$ | $\varepsilon_{nom}$ | $\sigma_{true}$ | $\varepsilon_{ln}^{pl}$ |
|------|------|------|------|
| 435 | 0.002197 | 408.3766 | 0 |
| 435 | 0.018269 | 415.3681 | 0.015867 |
| 499.3333 | 0.061538 | 502.4825 | 0.057042 |
| 523.3333 | 0.111731 | 554.2267 | 0.10298 |
| 523.3333 | 0.186731 | 593.4767 | 0.168066 |

Table 5 Stress -Strain values for Plate 3

| $\sigma_{nom}$ | $\varepsilon_{nom}$ | $\sigma_{true}$ | $\varepsilon_{ln}^{pl}$ |
|------|------|------|------|
| 436 | 0.00218 | 409.3715 | 0 |
| 436 | 0.011538 | 413.4517 | 0.009267 |
| 506.6667 | 0.065385 | 512.2158 | 0.060637 |
| 526.6667 | 0.105769 | 554.7928 | 0.097629 |
| 526.6667 | 0.186538 | 597.3312 | 0.167916 |

Table 6 Stress -Strain values for Plate 4

| $\sigma_{nom}$ | $\varepsilon_{nom}$ | $\sigma_{true}$ | $\varepsilon_{ln}^{pl}$ |
|------|------|------|------|
| 431 | 0.002155 | 404.3498 | 0 |
| 431 | 0.013077 | 409.0571 | 0.010809 |
| 510 | 0.061538 | 513.8056 | 0.057012 |
| 526 | 0.088462 | 544.9517 | 0.081903 |
| 526 | 0.146154 | 575.2979 | 0.133397 |

Table 7 Stress -Strain values for Plate 6

| $\sigma_{nom}$ | $\varepsilon_{nom}$ | $\sigma_{true}$ | $\varepsilon_{ln}^{pl}$ |
|------|------|------|------|
| 431 | 0.002113 | 404.3315 | 0 |
| 431 | 0.009615 | 407.5652 | 0.007436 |
| 483.3333 | 0.046154 | 478.062 | 0.042642 |
| 520 | 0.1 | 544.421 | 0.092506 |
| 520 | 0.176923 | 584.421 | 0.159903 |

### III.3 Geometric Imperfections

Since the verification test case considered in this part of
the study involves minor principal axis flexure of an I-
shaped beam under the action of pure moment,
bifurcation related response must be considered as a
possible factor governing overall response. When
applying the finite element method to bifurcation-type
stability problems, it is oftentimes advisable to
incorporate a reasonable imperfection field into the finite
element model. The incorporation of the imperfection
field is used to perturb the model from the condition of
perfect geometry; failure to do this may result in the
model artificially persisting in the perfect state
throughout the loading history. The potential proximity

of the finite element displacement solution to an initial perfect geometry arises since such a configuration is a mathematically admissible equilibrium state (even post bifurcation). However this configuration is meaningless physically since the slightest loading disturbance, or geometric imperfection, would render such an equilibrium state inaccessible to practical cases. As a means of guarding against any potentially physically aberrant response, a reasonable displacement-based imperfection field should be incorporated into finite element models whose response has the potential of being governed by bifurcation buckling. In such cases, it is not imperative that the precise governing buckling mode be used as an initial imperfection adopted at the start of the nonlinear solution. Rather, any imperfection field used need only possess elements of the dominant features that are contained in the governing mode. In the present verification study, it is observed from linearized eigenvalue buckling analyses, carried out with ABAQUS, that the governing mode of instability in minor axis I-shaped members in pure bending involves localized buckling within the flange. The perfect geometry was seeded with sinusoidally varying imperfection given by equation

$$w_o = A \, y \sin(\frac{\pi x}{L})$$

In the finite element analogs of the experimental test specimens, a reasonable displacement-based imperfection field is incorporated into the finite element models in the form of sinusoidally varying imperfection possessing a half wavelength of $B_f / 2$, that is phase shifted by 180 degrees between opposite flange tips (see figure 5) as well as a maximum displacement amplitude equal to 0.2 times the flange thickness or $B_f / 100$.
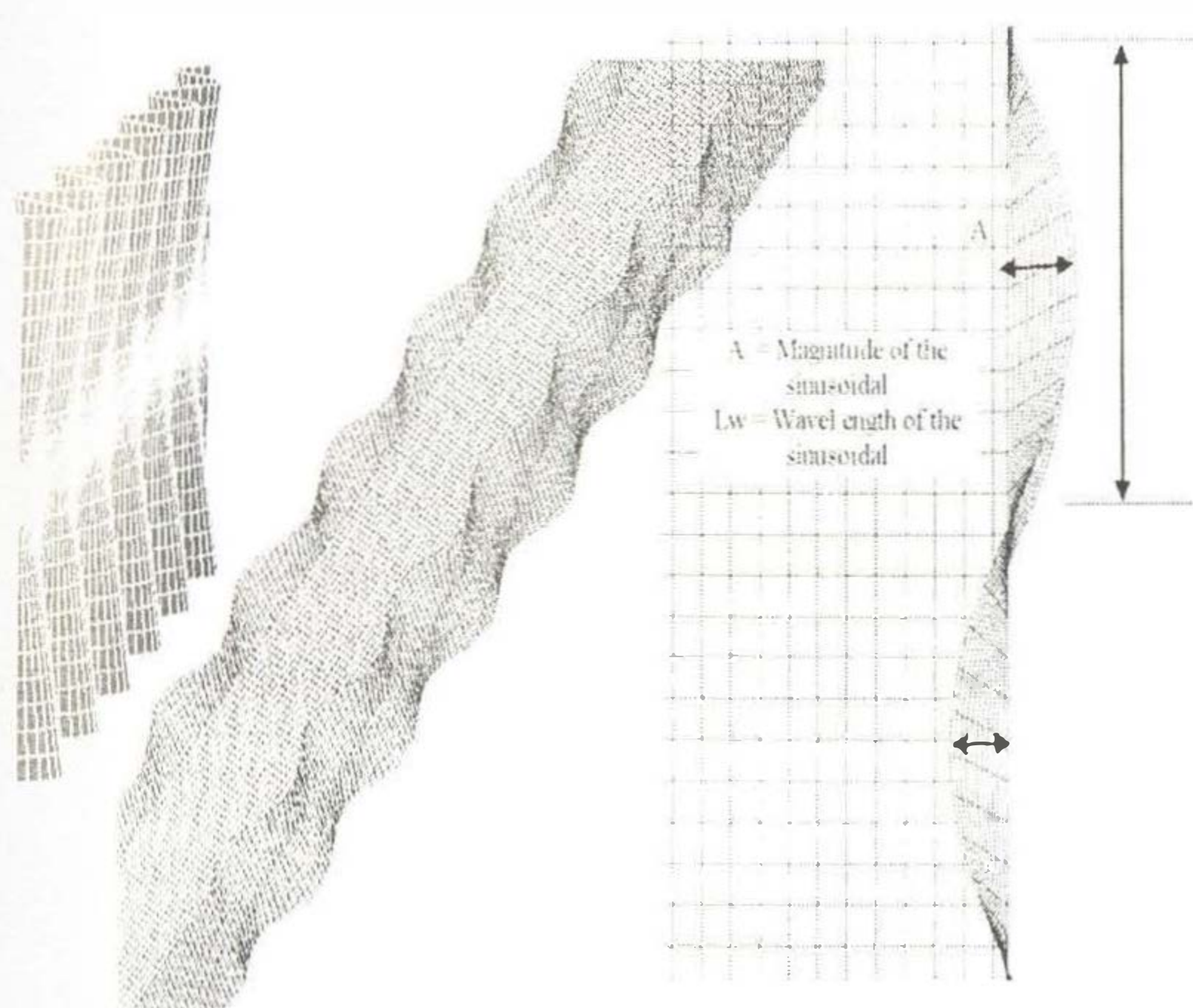


Figure 5 Sinusoidal imperfection

## IV. FINITE ELEMENT MODEL

*Finite element mesh:* The I-shaped cross-sections are built-up using S4R shell finite elements from ABAQUS element library positioned along the middle surfaces of the cross-sectional constituent plate components (fig 7).

While there is also moment gradient loading being applied at both rigid end segments, these end segments are not of interest in this research; that is why they are modeled as being approximately rigid through the use of and elastic modulus that is one order of magnitude higher than that of middle segment. Imperfections were applied only on the flanges. In addition, the rigid segments were not seeded with imperfections, and mesh densities used throughout the entire length of the beam were constant and uniform.

*Boundary Conditions:* The model is a simple supported beam. However; restraint against torsion is applied at the flange tips at the flexible-rigid transition interfaces. At the end of the I-shaped member, along the plate edges, rigid beam elements from the ABAQUS element library are employed to assist with maintaining ideal kinematics at points associated with the imposition of boundary conditions.

*Loading:* A constant moment loading is achieved by applying four concentrated forces perpendicular to the beam longitudinal axis. Axial loads are applied at the nodes at the roller end of the simply supported beam. In figure 6 test layout and finite element model representing the test is given in detail.

### IV.1 Verification of Test Results and Discussion

Results from seven of the experimental specimens reported from the research program of Rasmussen and Chick (1995) are compared with equivalent finite element models. Plots comparing these interaction responses appear in figures 8 and 9. In these figures, the maximum inelastic moment at the mid-span versus the axial load are plotted. The maximum moment is calculated as the sum of the end moment and the moment produced by the eccentricity of the axial force; $M = M_{end} + P\delta$ where $\delta$ is the mid-span deflection (i.e. the sum of the primary and secondary moments). Based on these results, it appears that the present modeling techniques are sufficiently robust to undertake the desired parametric study. Rasmussen and Chick [10] also reported the maximum axial force and corresponding second order moment values at the end points. It is noted that the format of these test results allows for an easy comparison with the design interaction curve in AISC-LRFD since it is defined in terms of ultimate axial load $(P_u)$ versus second order elastic moment $(M_{meu})$. In order to compare the experimental results with design interaction equations, end moment must be converted to second order moments. This can be done by using the following equation;

$$M_{meu} = B_1 \times M_{endu} \qquad\qquad B_1 = \frac{1}{1 - \frac{P_u}{P_e}}$$

where Euler buckling load is $P_e = \dfrac{\pi^2 EI}{L^2}$ ; a value enforced to be the flexural buckling load about the minor principal axis in this context, and $M_{endu}$ is the first order end moment coinciding with the controlling value of $P_u$.
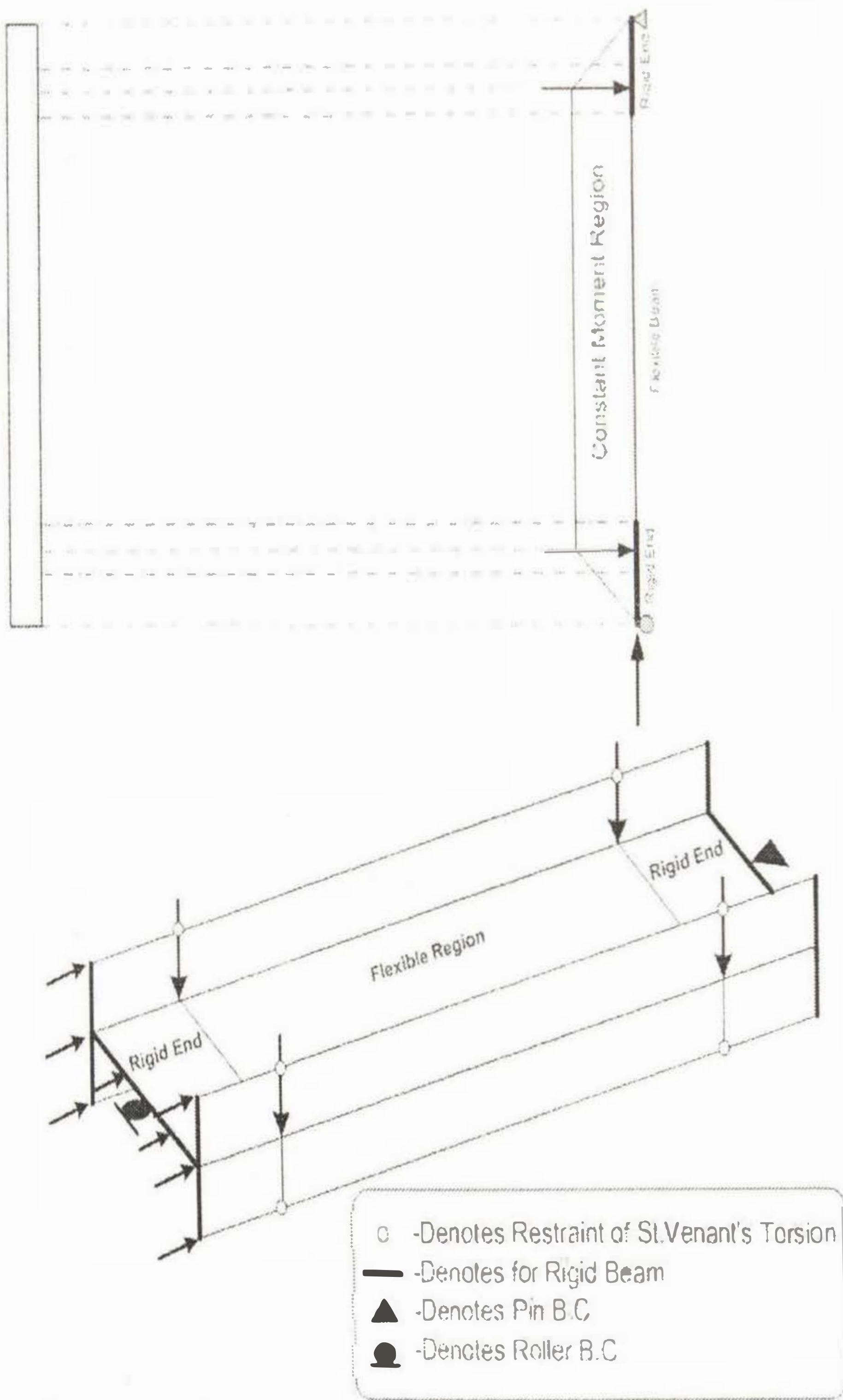
Furthermore, $M_{endu}$ from the ABAQUS results is converted into $M_{meu}$ and compared with the corresponding values given by Rasmussen and Chick[10]. Comparison of these values can be seen in table 8. Based on results from figure 8 and 9 as well as the failure loads presented in table 8, it appears that the present modeling techniques are sufficiently robust to undertake the current research work investigating combined loading response of I-shaped steel cross-sections bent about the minor-axis in the presence of axial compressive loading.

Table 8 Comparison of ultimate axial load and second order elastic moments

| Specimen | $P_u$ (kN) | | $M_{meu}$ (kNm) | |
|----------|------|------|------|------|
| | FEA | Test | FEA | Test |
| 3500-2 | 654.00 | 653.00 | 9.82 | 9.80 |
| 3500-3 | 536.28 | 553.00 | 14.75 | 15.60 |
| 3500-4 | 449.12 | 427.00 | 20.11 | 18.80 |
| 3500-5 | 63.97 | 65.00 | 40.79 | 41.50 |
| | | | | |
| 5800-2 | 414.51 | 430.00 | 5.99 | 7.30 |
| 5800-3 | 317.29 | 318.00 | 16.02 | 16.20 |
| 5800-4 | 191.85 | 181.00 | 28.78 | 26.30 |



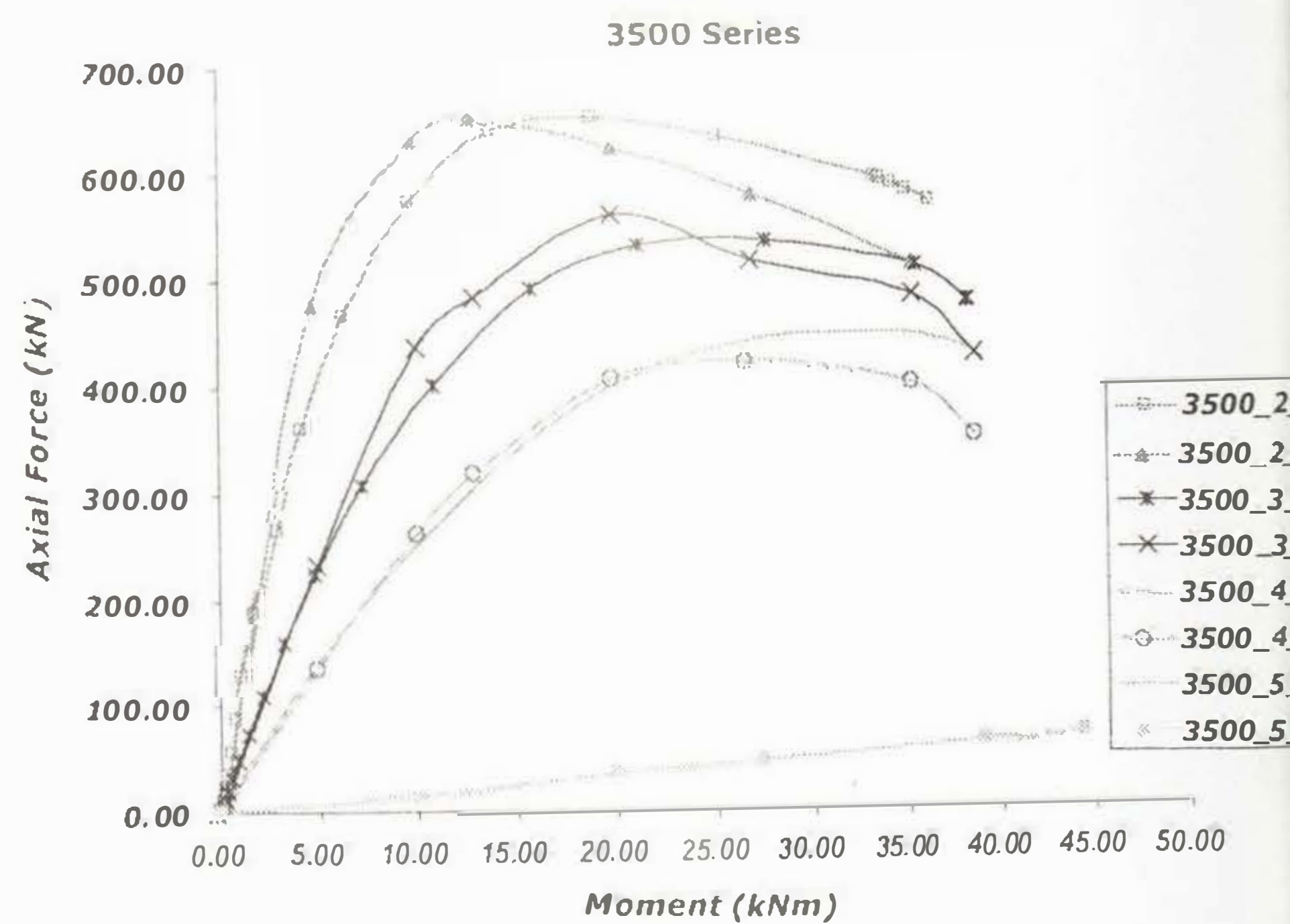Figure 6 Test rig and finite element modelling



Figure 8 Comparison of results for 3500 series



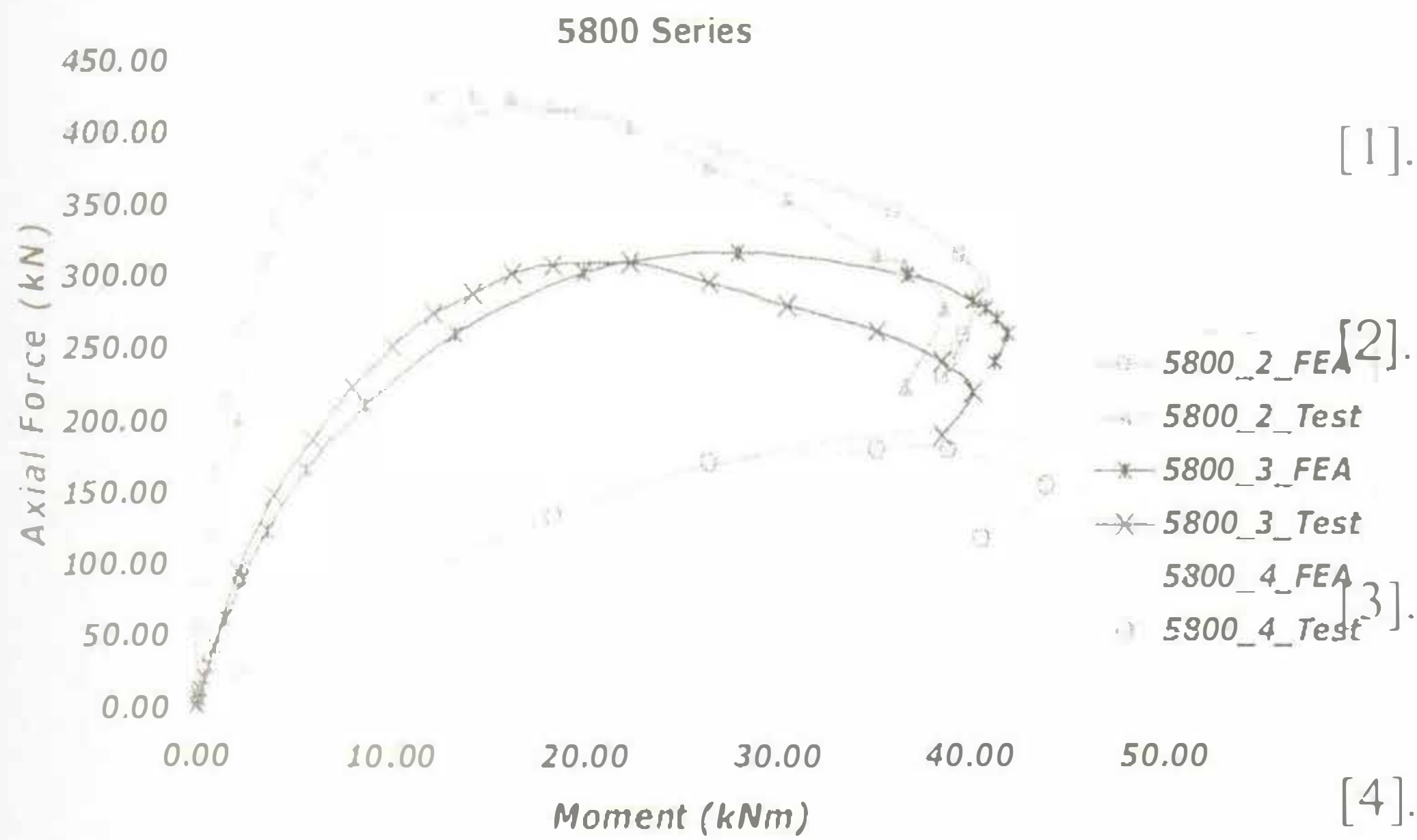Figure 7 Representative Shell Finite Element Mesh

Figure 9 Comparison of results for 5800 series

The differences between test results and numerical results arise from the fact that there are some uncertainties in both physical testing as well as finite element modeling. For the test specimens, stress strain properties, yield strength values of the material, and the plate geometry may be different through the section and along the beam length. Also mis-measured and reported initial geometric imperfections and residual stresses, unreported material properties, such as stress strain properties of material loaded in compression, do have important effects on the results of numerical models. Tension properties of the material are reported for the test specimen studied in this research. However, because of the Bauschinger affects, the tension behavior does not represent the compression behavior. In addition, as deformations become large, support and restraint conditions become critical and variability in these values can change the result dramatically.

## V. CONCLUSION

Results from finite element modelling techniques described in this paper can sufficiently catch the results of the real experiments. One has to understand the formulation or mathematical models used in the software package and then construct the model. Once the real lab test is verified then the parametric study can be carried out as desired. The important recommendations can be listed as:

1-General purpose shell element with reduced integratiom method catches the behavior of the structure under investigation.
2-Von-Mises yield model with isotropic hardening model works well for materials like steel.
3-Sinusoidally varying imperfection can be used to achieve the imperfect structure.

## BIBLIOGRAPHY

[1].   ABAQUS, (2001). "Users Manual," Version 6.3, Hibbitt, Karlsson & Sorenson, Inc., Pawtucket, Rhode Island, USA.
[2].   AISC, (1999). Load and Resistance Factor Design Specification for Structural Steel Buildings, 3rd Ed., American Institute of Steel Construction Inc., Chicago, Illinois.
[3].   Bathe, K.J., (1982). Finite Element Procedures in Engineering Analysis, Prentice Hall, Inc.. New Jersey.
[4].   Chacrabarty, J., (1987). Theory of Plasticity, McGraw-Hill Book Company.
[5].   Cook, R.D., Malkus, D.S. Plesha, M.E., (1989). Concepts and Application of Finite Element Analysis, 3rd edition, John Wiley & Sons, Inc., USA.
[6].   Galambos, T. V., (1998) Guide to Stability Design Criteria for Metal Structures, Fifth Edition, John Wiley & Sons, Inc., New York, New York.
[7].   Galambos, T. V., Ravindra, M. K. (1978). "Properties of Steel for Use in LRFD," Journal of the Structural Division, Vol. 104 , No. ST9, pp.1459-1468.
[8].   Greco, N., Earls, C.J., (2003). "Structural Ductility in Hybrid High Performance Steel Beams," Journal of Structural Engineering, Vol. 129, No. 12, American Society of Civil Engineers, Reston, Virginia, pp.1584-1595.
[9].   Ramm, E. Stegmuller, H.. (1982). "Buckling of Shells", Proceeding of a State of the Art Colloqium
[10].  Rasmussen, K.J.R. and Chick, C.G. (1995). "Tests of thin walled I-section in combined compression and minor axis bending- Part II-Proportional Loading Tests," The University of Sydney – School of Civil and Mining Engineering Research Report No.R717.
[11].  Thomas, S., Earls, C.J., (2003a) "Cross-sectional Compactness and Bracing Requirements for HPS483W Girders," Journal of Structural Engineering, Vol. 129, No. 12 American Society of Civil Engineers, Reston, Virginia, pp. 1569-1583